

RESEARCH ARTICLE | APRIL 17 2023

# Lateral charge migration in 1D semiconductor–metal hybrid photocatalytic systems

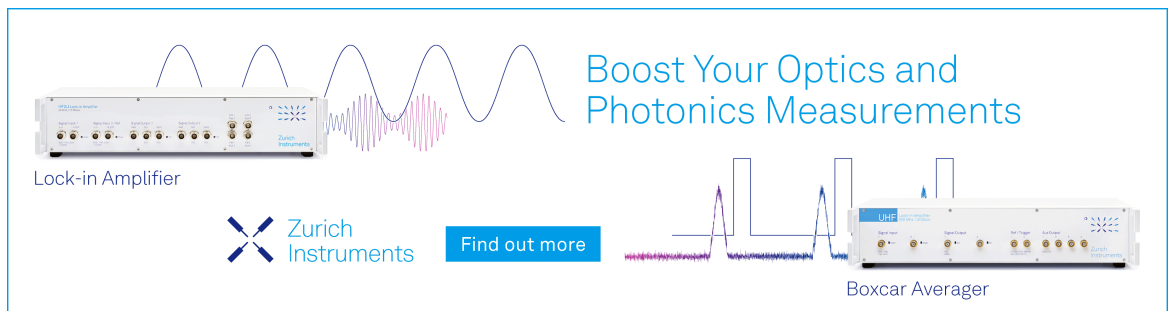
Special Collection: [40 Years of Colloidal Nanocrystals in JCP](#)

Mathias Micheel  ; Kaituo Dong  ; Lilac Amirav   ; Maria Wächtler  

 Check for updates


*J. Chem. Phys.* 158, 154701 (2023)

<https://doi.org/10.1063/5.0144785>



Boost Your Optics and Photonics Measurements

Lock-in Amplifier

 Zurich Instruments

[Find out more](#)

Boxcar Averager

# Lateral charge migration in 1D semiconductor–metal hybrid photocatalytic systems

Cite as: J. Chem. Phys. 158, 154701 (2023); doi: 10.1063/5.0144785

Submitted: 1 February 2023 • Accepted: 24 March 2023 •

Published Online: 17 April 2023



View Online



Export Citation



CrossMark

Mathias Micheel,<sup>1</sup>  Kaituo Dong,<sup>2</sup>  Lilac Amirav,<sup>2,a)</sup>  and Maria Wächtler<sup>1,3,a)</sup> 

## AFFILIATIONS

<sup>1</sup>Department Functional Interfaces, Leibniz-Institute of Photonic Technology Jena, Albert-Einstein-Straße 9, 07745 Jena, Germany

<sup>2</sup>Schulich Faculty of Chemistry, The Russell Berrie Nanotechnology Institute, The Nancy and Stephen Grand Technion Energy Program, Technion–Israel Institute of Technology, Haifa 32000, Israel

<sup>3</sup>Chemistry Department and State Research Center Optimas, RPTU Kaiserslautern-Landau, Erwin-Schrödinger-Straße 52, 67663 Kaiserslautern, Germany

**Note:** This paper is part of the JCP Special Topic on 40 Years of Colloidal Nanocrystals in JCP.

**a) Authors to whom correspondence should be addressed:** [lilac@technion.ac.il](mailto:lilac@technion.ac.il) and [maria.waechtler@chem.rptu.de](mailto:maria.waechtler@chem.rptu.de)

## ABSTRACT

Colloidal nanorods based on CdS or CdSe, functionalized with metal particles, have proven to be efficient catalysts for light-driven hydrogen evolution. Seeded CdSe@CdS nanorods have shown increasing performance with increasing rod length. This observation was rationalized by the increasing lifetime of the separated charges, as a large distance between holes localized in the CdSe seed and electrons localized at the metal tip decreases their recombination rate. However, the impact of nanorod length on the electron-to-tip localization efficiency or pathway remained an open question. Therefore, we investigated the photo-induced electron transfer to the metal in a series of Ni-tipped CdSe@CdS nanorods with varying length. We find that the transfer processes occurring from the region close to the semiconductor–metal interface, the rod region, and the CdSe seed region depend in different ways on the rods' length. The rate of the fastest process from excitonic states generated directly at the interface is independent of the rod length, but the relative amplitude decreases with increasing rod length, as the weight of the interface region is decreasing. The transfer of electrons to the metal tip from excitons generated in the CdS rod region depends strongly on the length of the nanorods, which indicates an electron transport-limited process, i.e., electron diffusion toward the interface region, followed by fast interface crossing. The transfer originating from the CdSe excitonic states again shows no significant length dependence in its time constant, as it is probably limited by the rate of overcoming the shallow confinement in the CdSe seed.

© 2023 Author(s). All article content, except where otherwise noted, is licensed under a Creative Commons Attribution (CC BY) license (<http://creativecommons.org/licenses/by/4.0/>). <https://doi.org/10.1063/5.0144785>

## INTRODUCTION

Semiconductor–metal hybrid, nanostructured, photocatalytic systems have been the focus of intense research due to their ability to support solar-to-fuel conversion.<sup>1–5</sup> In such hybrid systems, the semiconductor nanoparticle serves as a light-harvester, which transfers an electron to a metallic cocatalyst upon photoexcitation. Understanding the underlying charge carrier dynamics within the complete system is crucial for developing improved systems. In particular, the influence of the metal cocatalyst composition,<sup>6–11</sup>

size,<sup>12–15</sup> deposition site, and particle number<sup>16–20</sup> on the interfacial charge transfer and resulting photon-to-hydrogen efficiency has been investigated in detail during the past years. In comparison, charge carrier migration within the semiconductor component has received little attention. It is well established that for pure one-dimensional semiconductor systems, the semiconductor dimensions and surface quality influence the charge migration and localization.<sup>21–25</sup> However, the influence of these intrinsic charge carrier migration dynamics on the charge separation dynamics and efficiency in hybrid systems remains a relatively unexplored topic.

Hybrid systems, comprised of CdSe@CdS dot-in-rod particles functionalized with metallic nanoparticles, demonstrated high efficiency in converting protons to molecular hydrogen upon photoexcitation.<sup>2,26,27</sup> We previously found that the rate constant of electron transfer to the metal cocatalyst in such systems was independent of metal size<sup>12</sup> or composition,<sup>7</sup> whereas the charge separation and photocatalytic hydrogen production efficiency were highly sensitive to these parameters. In general, electron transfer in these hybrid systems originates from excitons localized at different locations within the rod, i.e., near the interface, near the CdSe core, or within the core, and occurs within  $\sim 100$  ps.<sup>7,12,28</sup> In contrast, the interface crossing from the semiconductor to the metal domain is expected to be much faster ( $< 1$  ps).<sup>15,29</sup> The independence of the observed electron transfer rate constant from the characteristics of the metal cocatalyst can thus be explained by a slower electron diffusion toward the tip, which precedes any interface crossing, and determines the observed rate. On the other hand, the efficiency of interface crossing is affected entirely by the semiconductor–metal interface. The efficiency of charge separation and the rate of proton reduction at the metal tip determine the catalytic efficiency.

Herein, we provide evidence that intra-rod electron diffusion can be the rate-determining step for electron transfer. We have investigated seeded nanorods of similar diameter ( $5.0 \pm 0.4$  nm) and identical metal cocatalyst composition and size (Ni,  $5.0 \pm 0.5$  nm),

while varying the rods' length in the range 20–60 nm. We used transient absorption spectroscopy to follow the photoinduced bleach recovery and electron dynamics, and determined how the electron transfer kinetics develops as a function of the rod's length. We discuss the implications of these findings for the future design of optimized nanoscale, photocatalytic, hybrid systems.

## RESULTS

Given the established influence of the rod's diameter and metal size<sup>12,22,30</sup> on the electronic structure and charge separation dynamics, respectively, it was vital to precisely control these characteristics, to enable proper studies on length dependent effects. The full protocols for CdSe@CdS rod synthesis and Ni tipping are published elsewhere,<sup>12,26</sup> and a full account of the synthetic protocols is included in the [supplementary material](#). Nanorods with varied length were obtained via adjustment of the amounts of the CdSe seed and ligands that were used in their synthesis. Alternative methods for length adjustments, such as variations in the reaction temperature or reaction time, were avoided, in an attempt to fix the rods' diameter. The well-controlled deposition of a Ni nanoparticle tip is based on the reduction of nickel(II) acetylacetonate as the nickel precursor by oleylamine and trioctyl phosphine.<sup>10</sup> Adjustment of the nickel precursor concentration, reaction temperature and time,

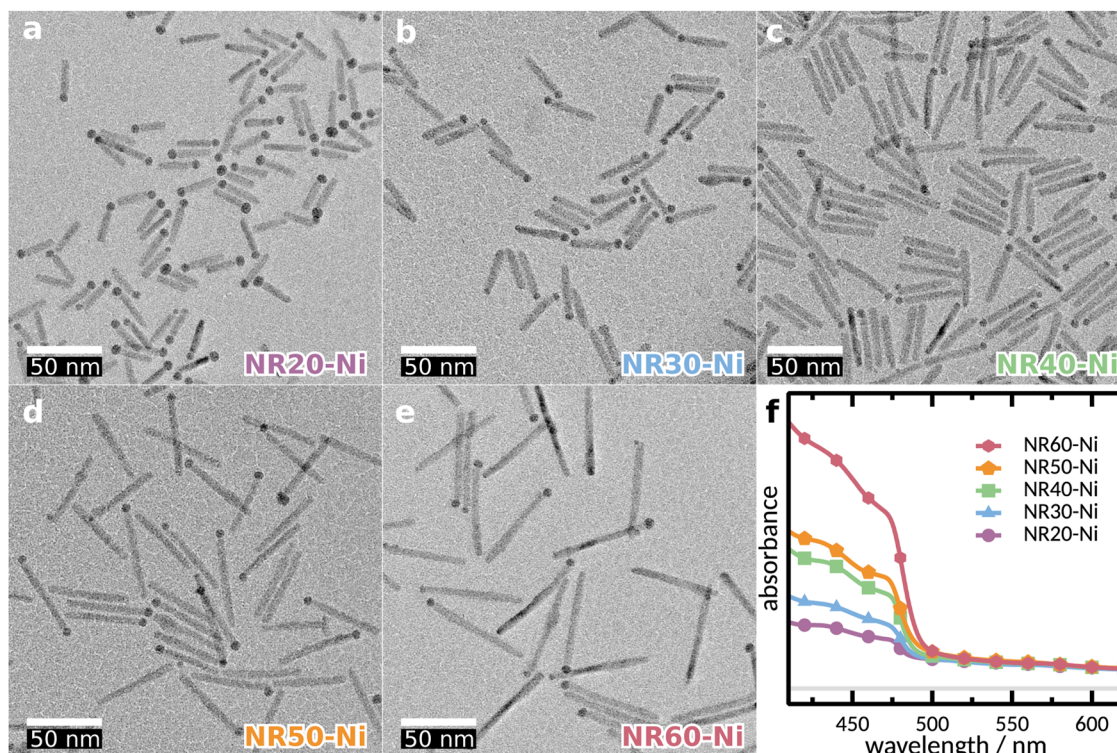


**FIG. 1.** Characterization of Ni-tipped CdSe@CdS nanorods. (a)–(e) TEM micrographs of the structures under investigation. (f) Absorption spectra of the tipped nanorods. All spectra have been normalized to the tip absorption at 625 nm. The TEM images and absorption spectra of non-functionalized samples can be found in the [supplementary material](#).

and the ligands that are used enables the desired control over the Ni nanoparticle size, location, and number of sites on the CdS rod surface. The Ni tip size was selected to be  $5.0 \pm 0.5$  nm, given that this size displayed the optimal photocatalytic activity toward hydrogen production.<sup>12</sup> Figure 1 shows transmission electron microscope (TEM) micrographs of the examined rods, with similar diameter and Ni tip size, and varying lengths. The detailed information on the dimensions (length, width, Ni-tip diameter), as well as the statistics for the number of metal domains per rod, is included in Table I. The samples were given abbreviated names, representing the rods' length, which are used throughout the paper (Table I).

Absorption spectra of all pure nanorods dispersed in toluene showed the characteristic excitonic transitions related to the CdS rod below 470 nm and the comparably minor CdSe seed absorption at c. 560 nm (Fig. S6).<sup>31,32</sup> The ratio of CdS:CdSe absorption becomes larger with increasing rod length because of the increasing CdS rod volume. Ni-tipped samples show additional broad absorption contribution spanning the entire visible spectrum due to scattering and absorption of light by the Ni nanoparticles [Fig. 1(f)].

Photoluminescence spectroscopy gives first insights into the nanorod–tip interaction. For the bare nanorods, we observe the band-edge emission of the CdSe core (recorded upon excitation of the CdS rod at 450 nm) between 530 and 630 nm (Fig. S7). Absolute photoluminescence quantum yields of bare rods are of the order of 0.5–0.8 (Table S2). Photoluminescence spectra of Ni-tipped samples are identical to their respective bare samples, but their quantum yields are drastically reduced to 0.1 and less. We attribute part of this residual emission to untipped nanorods, which are sometimes present in quantitative amounts (up to 20% for NR60-Ni), together with the tipped samples. Additionally, some residual emission that originates from metal tipped rods provides an inverse indication of the efficiency of interfacial charge crossing.<sup>12,33</sup> Given the optimization of the Ni domain size, which was designed to maximize the probability for charge separation, the contribution to the emission by metal tipped rods, in this case, is minimal. Indeed, once we correct for the fraction of non-functionalized nanorods, the quenching efficiency for all tipped rods is close to unity (see the supplementary material for a detailed description). This confirms that charge-separation of the photogenerated exciton competes very efficiently with radiative recombination: While the hole ultimately localizes to the CdSe core, the electron is transferred to the Ni tip.<sup>12,34</sup>

Charge transfer to the cocatalyst in metal–semiconductor hybrid systems occurs within several tens of picoseconds and faster.

Thus, we investigated the charge separation kinetics on a sub-2 ns-timescale via transient absorption spectroscopy with sub-100 fs time resolution. Transient absorption spectroscopy is sensitive to the population of conduction band states in photoexcited nanostructures and delivers information on electron dynamics.<sup>22,31,35</sup> Samples were excited at 390 nm, i.e., the CdS rods, and probed with a supercontinuum spanning from 350 to 750 nm. Transient spectra recorded for bare nanorods show the characteristic bleach features of the CdS rod excitonic transition between 460 and 480 nm and the CdSe core excitonic transition between 530 and 600 nm, due to state filling of the conduction band levels (Figs. S8–S12).<sup>36</sup>

As expected, the CdS bleach recovery is substantially accelerated in the Ni functionalized samples, compared to the bare samples [Fig. 2(a)] and is complete within several hundred picoseconds. We assign the accelerated bleach recovery to the interfacial electron transfer from the CdS rod conduction band states to the Ni tip. To gain a quantitative understanding of the temporal and spectral evolution of the transient spectra, they were subjected to a global fit. Our model accounts for the presence of bare rods, together with the tipped rods (see Table I), and for tipped nanorods that do not undergo charge separation, Refs. 12 and 37, in the region 400–500 nm, reflecting on the bleach of CdS localized excitonic transitions. We modeled the accelerated bleach recovery of tipped rods with two time constants ( $\tau_{\text{ET},1}$  and  $\tau_{\text{ET},2}$ ), which reflect the electron transfer to the Ni tip. In addition, we separately modeled the CdS bleach dynamics in non-functionalized samples by four time constants (Table II). A complete discussion of these time constants for non-functionalized samples can be found in the supplementary material. In the following, we solely focus on the discussion of the length dependence of the electron transfer process.

The first time constant,  $\tau_{\text{ET},1}$ , is for the functionalized samples of the order of 0.2 ps for all samples, irrespective of their length. A similarly fast process on a timescale of hundreds of fs has previously been observed for metal-tipped CdSe@CdS, CdSe, and CdS nanorods,<sup>15,28,29</sup> and has been attributed to a “hot” electron transfer. In such cases, the electron transfer to the tip precedes any intra-band relaxations to the band-edge. The second time constant,  $\tau_{\text{ET},2}$ , is of the order of few to tens of ps and corresponds to the CdS band-edge electron transfer to the Ni tip.<sup>12</sup> “Band-edge electron” refers, in this context, to electrons that are localized in a distant part of the nanorod (relative to the metal tip), i.e., close to the CdSe core, but still within the CdS rod. This process is, in principle, in competition with the slightly faster rod-to-seed exciton localization, but the

**TABLE I.** Overview of the investigated CdSe@CdS nanorods. Indicated are the rod length and width, as well as the Ni-tip diameter. For the tipped samples, we also indicated the amount of untipped (0T), single-tipped (1T), and double-tipped (2T) rods present in the sample mixture.

Bare sample	Length (nm)	Width (nm)	Ni-tipped samples	Tip diameter (nm) (0T-1T-2T) (%)
NR20	$19.7 \pm 1.6$	$5.0 \pm 0.4$	NR20-Ni	$4.7 \pm 0.3$ (3-88-9)
NR30	$30.0 \pm 2.0$	$5.4 \pm 0.5$	NR30-Ni	$4.5 \pm 0.6$ (10-83-7)
NR40	$40.1 \pm 3.1$	$5.3 \pm 0.6$	NR40-Ni	$4.8 \pm 0.5$ (12-82-6)
NR50	$51.5 \pm 3.5$	$4.6 \pm 0.5$	NR50-Ni	$4.8 \pm 0.6$ (13-82-6)
NR60	$60.7 \pm 4.6$	$5.4 \pm 0.5$	NR60-Ni	$5.5 \pm 0.8$ (20-80-1)

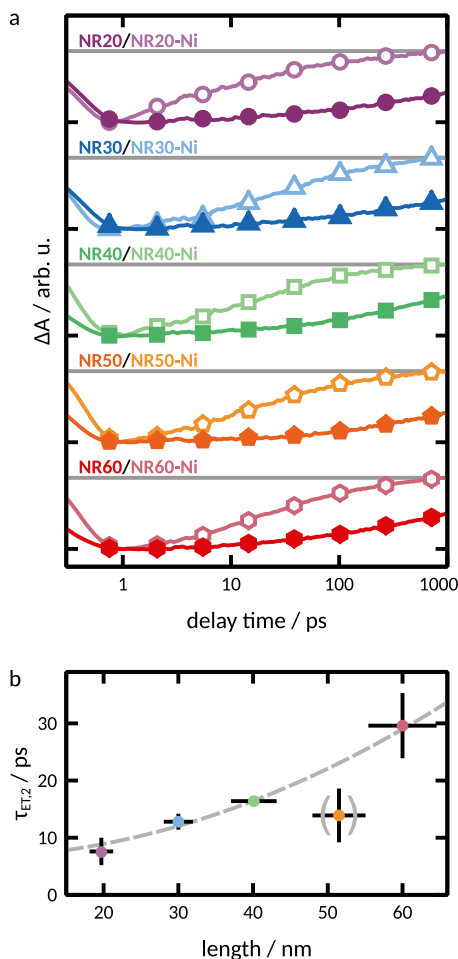


**FIG. 2.** Transient absorption spectroscopy of pure and hybrid structures. (a) Normalized kinetics of the CdS bleach recovery at 460 nm of bare (filled symbols) and functionalized (open symbols) nanorods. To obtain pure kinetic traces for functionalized nanorods, without contributions of residual bare rods, the bare nanorod kinetics, normalized at 1000 ps, was subtracted from the as-measured kinetics of the functionalized samples. (b) Determined CdS conduction band electron transfer lifetimes ( $\tau_{ET,2}$ ) as a function of rod length. The dashed line represents a quadratic fit of the data excluding NR50-Ni.

localization process does not occur with 100% efficiency, which is always observable.<sup>21,22</sup> As clearly seen in Fig. 2(b),  $\tau_{ET,2}$  increases with increasing the rod length from  $\tau_{ET,2} = 7.6 \pm 2.4$  ps for the NR20-Ni sample to  $\tau_{ET,2} = 29.6 \pm 5.7$  ps for the NR60-Ni sample. Electron transfer in NR50-Ni was found to be substantially faster than expected compared to the trend indicated by the other samples. This deviation from the general trend may be ascribed to the nanorod width, which is smaller than that of the other nanorods. The CdS diameter affects the intrinsic underlying electronic structure of the nanorod and, accordingly, the electron dynamics.<sup>30</sup>

The accelerated CdSe bleach decay was quantified in the spectral region 530–610 nm in a similar manner. Here, a single time constant was required to describe the accelerated decay compared

**TABLE II.** Time-constants of electron transfer in tipped CdSe@CdS, obtained via global fitting of the CdS and CdSe bleach regions. Time constants of the non-functionalized nanorods can be found in the [supplementary material](#) (Tables S3 and S4).

Sample	$\tau_{ET,1}$ (ps)	$\tau_{ET,2}$ (ps)	$\tau_{ET,CdSe}$ (ps)
NR20-Ni	$0.3 \pm 0.1$	$7.6 \pm 2.4$	$45 \pm 17$
NR30-Ni	$0.2 \pm 0.1$	$12.8 \pm 1.4$	$59 \pm 4$
NR40-Ni	$0.3 \pm 0.1$	$16.4 \pm 0.7$	$71 \pm 10$
NR50-Ni	$0.3 \pm 0.1$	$13.9 \pm 4.7$	$25 \pm 11$
NR60-Ni	$0.2 \pm 0.1$	$29.6 \pm 5.7$	$54 \pm 4$

to the bare rods, and without considerable changes between samples. It was determined to be of the order of  $\tau_{ET,CdSe} = (60 \pm 10)$  ps. Again, NR50-Ni showed a faster bleach recovery, presumably due to its smaller width, and should not be considered in the discussion here. In quasi-type II nanostructures, the electron is delocalized over the entire structure, yet with higher probability around the CdSe core. Hence, the CdSe bleach is representative of the conduction band electron population situated close to, and in the core. The time constant,  $\tau_{ET,CdSe}$ , thus represents electron transfer from excitonic states localized in or near the CdSe seed.<sup>12</sup>

## DISCUSSION

The goal of this study was to shed light on the electron transfer mechanism in one-dimensional, semiconductor–metal hybrid systems. In accordance with the previous literature reports, we identified three distinct time regimes of electron transfer, which we can relate to the structure of the hybrid system. First, we observed a very fast ( $\tau_{ET,1} \ll 1$  ps) hot electron transfer to the metal tip that is independent of the rod’s length. We want to emphasize that the determined lifetime of  $\tau_{ET,1}$  is limited by our experimental time resolution of  $\sim 100$  fs. This process occurs on the same or even shorter timescale than the dissociation of the exciton that is followed by hole localization to the CdSe core (as indicated by  $\tau_2$  in the bare rods). Hence, we interpret this as interfacial electron transfer, occurring directly from a photogenerated exciton that is generated in the CdS rod in close proximity to the Ni tip. The time constant for such direct interfacial charge crossing is not expected to be sensitive to the rod’s length, in accordance with our observations. An analysis of the corresponding amplitudes of both electron transfer steps shows that the relative contribution of this hot electron transfer to the bleach recovery varies and is inversely proportional to the rod length ([supplementary material](#)). Additional influences that might be caused by varying barrier heights are related to changes in the nickel particle’s size, and, thus, may be neglected here, given that all rods possess similar-sized Ni tips. This amplitude accounts for  $\sim 70\%$  of the bleach recovery for NR20-Ni and drops to  $\sim 50\%$  for NR60-Ni. These trends further support our assignment of  $\tau_{ET,1}$  to the interfacial electron transfer, as this process becomes more probable with a shorter distance from the location of exciton formation to the metal tip. In other words, with decreasing the rod’s length, the probability of photogeneration of an exciton, in sufficient proximity to the interface, increases.

On the other hand, the CdS band-edge electron transfer (as expressed in  $\tau_{ET,2}$ ), of the order of several ps, becomes slower with increasing rod length, which indicates that electron diffusion to the metal tip is the rate determining step in this charge transfer process. The relationship between  $\tau_{ET,2}$  and the rod's length is successfully approximated with a quadratic fit, which represents the one-dimensional electron diffusion,<sup>22</sup> and yields a diffusion constant of the order of  $\sim 10^{-4} \text{ m}^2 \text{ s}^{-1}$ . Even though our simplistic approach ignores additional electron decay pathways, such as localization or trapping, which may occur on a similar timescale, this value is in good accordance with the determined value for electron diffusion in non-functionalized CdSe@CdS nanorods of  $2.4 \times 10^{-4} \text{ m}^2 \text{ s}^{-1}$ .<sup>22</sup> While this estimation for non-functionalized rods is based on localization efficiencies derived from steady-state photoluminescence spectroscopy, the diffusion constant obtained for Ni-tipped rods in the present work stems from actual fitting of the time constants.

Finally, we observed the transfer of electrons that are situated near the CdSe core and whose time constant  $\tau_{ET,CdSe}$  ( $\sim 60 \pm 10$  ps) is again independent of the rod's length. For all samples investigated, this process is significantly slower than the diffusion-controlled, band-edge electron transfer ( $\tau_{ET,2}$ ). Because the metal particle preferentially grows at the (001) facet of the CdS rod,<sup>38</sup> i.e., the rod tip farthest away from the CdSe seed,<sup>39</sup> it is surprising that  $\tau_{ET,CdSe}$  does not similarly depend on the rod dimensions as  $\tau_{ET,2}$  does. A plausible explanation for this result is that overcoming the shallow confinement of the electron to the CdSe core region, due to the rod's quasi-type II electronic structure, is the rate-determining step in this electron transfer process, whereas the diffusion toward the tip is relatively faster.

## CONCLUSION

These results manifest into generalized design principles for one-dimensional, photocatalytic, semiconductor–metal systems. Interfacial electron crossing to the metal catalyst is significantly faster than any electron diffusion and is not the rate-determining step for charge separation. Yet, we found that the relative efficiency of the interfacial hot electron transfer slightly decreases with increasing the rod's length. In contrast, electron transfer from CdS-localized, band-edge states is highly sensitive to the nanorod's dimensions. Choi *et al.* recently emphasized the complicated relation between reduced electron transfer rates and increased absorption coefficients with increasing rod length in Pt-tipped CdSe nanorods.<sup>40</sup> They deduced an optimal nanorod length of  $\sim 20$  nm; a length scale at which dot-in-rod hybrid systems perform worse than pure nanorods.<sup>28,41</sup> On the other hand, CdSe@CdS–Pt nanorods showed significantly improved hydrogen generation quantum efficiency upon increasing the rod's length from 20 to 70 nm.<sup>42</sup> Our findings deliver a mechanistic explanation for this. Even though electron transfer from CdS band-edge states is diffusion controlled, electron diffusion to the semiconductor–metal interface is still sufficiently fast to outcompete recombination processes up to lengths of at least 60 nm and, hence, is not limiting the electron transfer to the metal tip. Wu *et al.* previously estimated the optimal rod length for photocatalysis to be  $\sim 100$  nm, based on the rod-to-seed localization efficiency in non-functionalized dot-in-rods.<sup>22</sup> Extrapolation of the electron transfer times in Fig. 2(b) to this rod

length yields an electron transfer time constant of  $\sim 70$  ps (see the [supplementary material](#) for details), which is still substantially faster than other electron trapping and recombination pathways. Electron diffusion, accordingly, still occurs efficiently even at such long lengths. This emphasizes the integral role of the dot-in-rod design investigated here, in which the CdSe seed supports orders of magnitude longer electron–hole separation compared to that of unseeded rods.<sup>7,43</sup> In short, we presented a simple framework for optimized semiconductor–metal hybrid, nanostructured, photocatalytic system design toward efficient photocatalytic reactions such as water splitting.

## SUPPLEMENTARY MATERIAL

The [supplementary material](#) includes detailed information of the synthetic protocols and sample characterization, with information on the methodologies utilized. The supplementary material is available free of charge on the website.

## DEDICATION

This work was dedicated to Professor Wolfgang Weigand on the occasion of his 65th birthday.

## ACKNOWLEDGMENTS

This research was supported, in part, by a grant from the German-Israeli Foundation for Scientific Research and Development (GIF, Grant No. G-1535-500.15/2021). Furthermore, the financial support by the German Research Foundation (DFG) under Project No. 364549901 – TRR234 (CataLight, B4) and the Fonds der Chemischen Industrie (FCI) is acknowledged (M.W.). L.A. and K.D. acknowledge the support from the Marie Skłodowska–Curie Actions of the European H2020 program MSCA-ITN-2016 (Grant Agreement No. 722591-PHOTOTRAIN), and the support of the Israeli Ministry of National Infrastructures, Energy and Water Resources (Grant No. 218-11-044). Furthermore, we thank Bei Liu for the support in the preparation of samples for the TA measurements.

## AUTHOR DECLARATIONS

### Conflict of Interest

The authors have no conflicts to disclose.

### Author Contributions

**Mathias Micheel:** Conceptualization (equal); Data curation (equal); Formal analysis (equal); Investigation (equal); Methodology (equal); Validation (equal); Visualization (equal); Writing – original draft (equal); Writing – review & editing (equal). **Kaituo Dong:** Conceptualization (equal); Formal analysis (equal); Investigation (equal); Methodology (equal). **Lilac Amirav:** Conceptualization (equal); Data curation (equal); Funding acquisition (equal); Methodology (equal); Project administration (equal); Resources (equal); Supervision (equal); Writing – review & editing (equal). **Maria Wachtler:**

Conceptualization (equal); Data curation (equal); Formal analysis (equal); Funding acquisition (equal); Methodology (equal); Project administration (equal); Resources (equal); Supervision (equal); Writing – review & editing (equal).

## DATA AVAILABILITY

Spectroscopic data, including the absorption, photoluminescence, and transient absorption spectroscopy that support the findings of this study, are openly available at Zenodo at <https://doi.org/10.5281/zenodo.7680636>, Ref. 44.

## REFERENCES

- N. Waikopf, Y. Ben-Shahar, and U. Banin, *Adv. Mater.* **30**, 1706697 (2018).
- K. Wu and T. Lian, *Chem. Soc. Rev.* **45**, 3781 (2016).
- R. Burke, K. L. Bren, and T. D. Krauss, *J. Chem. Phys.* **154**, 030901 (2021).
- P. Moroz, A. Boddy, and M. Zamkov, *Front. Chem.* **6**, 353 (2018).
- N. Razgoniaeva, P. Moroz, S. Lambright, and M. Zamkov, *J. Phys. Chem. Lett.* **6**, 4352 (2015).
- P. Kalisman, L. Houben, E. Aronovitch, Y. Kauffmann, M. Bar-Sadan, and L. Amirav, *J. Mater. Chem. A* **3**, 19679 (2015).
- M. Wächtler, P. Kalisman, and L. Amirav, *J. Phys. Chem. C* **120**, 24491 (2016).
- K. Dong, Q.-C. Chen, Z. Xing, Y. Chen, Y. Qi, N. G. Pavlopoulos, and L. Amirav, *Chem. Mater.* **33**, 6394 (2021).
- E. Aronovitch, L. Houben, and M. Bar-Sadan, *Chem. Mater.* **31**(18), 7231–7237 (2019).
- Y. Nakibli and L. Amirav, *Chem. Mater.* **28**, 4524 (2016).
- E. Aronovitch, P. Kalisman, S. Mangel, L. Houben, L. Amirav, and M. Bar-Sadan, *J. Phys. Chem. Lett.* **6**, 3760 (2015).
- Y. Nakibli, Y. Mazal, Y. Dubi, M. Wächtler, and L. Amirav, *Nano Lett.* **18**, 357 (2018).
- Y. Liu, W. Yang, Q. Chen, D. A. Cullen, Z. Xie, and T. Lian, *J. Am. Chem. Soc.* **144**, 2705 (2022).
- Y. Ben-Shahar, F. Scotognella, I. Kriegel, L. Moretti, G. Cerullo, E. Rabani, and U. Banin, *Nat. Commun.* **7**, 10413 (2016).
- Y. Ben-Shahar, J. P. Philbin, F. Scotognella, L. Ganzer, G. Cerullo, E. Rabani, and U. Banin, *Nano Lett.* **18**, 5211 (2018).
- T. Simon, M. T. Carlson, J. K. Stolarczyk, and J. Feldmann, *ACS Energy Lett.* **1**, 1137 (2016).
- Y. Nakibli, P. Kalisman, and L. Amirav, *J. Phys. Chem. Lett.* **6**, 2265 (2015).
- J. U. Bang, S. J. Lee, J. S. Jang, W. Choi, and H. Song, *J. Phys. Chem. Lett.* **3**, 3781 (2012).
- M. Karakus, Y. Sung, H. I. Wang, Z. Mics, K. Char, M. Bonn, and E. Cánovas, *J. Phys. Chem. C* **121**, 13070 (2017).
- Y. Sung, J. Lim, J. H. Koh, L. J. Hill, B. K. Min, J. Pyun, and K. Char, *CrystEngComm* **17**, 8423 (2015).
- M. Micheel, B. Liu, and M. Wächtler, *Catalysts* **10**, 1143 (2020).
- K. Wu, L. J. Hill, J. Chen, J. R. McBride, N. G. Pavlopoulos, N. E. Richey, J. Pyun, and T. Lian, *ACS Nano* **9**, 4591 (2015).
- M. D. Peterson, L. C. Cass, R. D. Harris, K. Edme, K. Sung, and E. A. Weiss, *Annu. Rev. Phys. Chem.* **65**, 317 (2014).
- V. L. Bridewell, R. Alam, C. J. Karwacki, and P. V. Kamat, *Chem. Mater.* **27**, 5064 (2015).
- K. Wu, W. Rodríguez-Córdoba, and T. Lian, *J. Phys. Chem. B* **118**, 14062 (2014).
- P. Kalisman, Y. Nakibli, and L. Amirav, *Nano Lett.* **16**, 1776 (2016).
- A. Agosti, Y. Nakibli, L. Amirav, and G. Bergamini, *Nano Energy* **70**, 104510 (2020).
- K. Wu, Z. Chen, H. Lv, H. Zhu, C. L. Hill, and T. Lian, *J. Am. Chem. Soc.* **136**, 7708 (2014).
- F. V. A. Camargo, Y. Ben-Shahar, T. Nagahara, Y. E. Panfil, M. Russo, U. Banin, and G. Cerullo, *Nano Lett.* **21**, 1461 (2021).
- T. Rosner, N. G. Pavlopoulos, H. Shoyhet, M. Micheel, M. Wächtler, N. Adir, and L. Amirav, *Nanomaterials* **12**, 3343 (2022).
- K. Wu, W. E. Rodríguez-Córdoba, Z. Liu, H. Zhu, and T. Lian, *ACS Nano* **7**, 7173 (2013).
- M. G. Lupo, F. Della Sala, L. Carbone, M. Zavelani-Rossi, A. Fiore, L. Lüer, D. Polli, R. Cingolani, L. Manna, and G. Lanzani, *Nano Lett.* **8**, 4582 (2008).
- L. Amirav and A. P. Alivisatos, *J. Am. Chem. Soc.* **135**, 13049 (2013).
- M. Zhukovskiy, P. Tongying, H. Yashan, Y. Wang, and M. Kuno, *ACS Catal.* **5**, 6615 (2015).
- D. P. Morgan and D. F. Kelley, *J. Phys. Chem. C* **124**, 8448 (2020).
- Q. Li, W. Yang, and T. Lian, in *Springer Handbook of Inorganic Photochemistry*, edited by D. Bahnemann and A. O. T. Patrocínio (Springer International Publishing, Cham, 2022), pp. 985–1012.
- A. Schleusener, M. Micheel, S. Benndorf, M. Rettenmayr, W. Weigand, and M. Wächtler, *J. Phys. Chem. Lett.* **12**, 4385 (2021).
- S. E. Habas, P. Yang, and T. Mokari, *J. Am. Chem. Soc.* **130**, 3294 (2008).
- D. V. Talapin, J. H. Nelson, E. V. Shevchenko, S. Aloni, B. Sadtler, and A. P. Alivisatos, *Nano Lett.* **7**, 2951 (2007).
- J. Y. Choi, W.-W. Park, B. Park, S. Sul, O.-H. Kwon, and H. Song, *ACS Catal.* **11**, 13303 (2021).
- F. Qiu, Z. Han, J. J. Peterson, M. Y. Odoi, K. L. Sowers, and T. D. Krauss, *Nano Lett.* **16**, 5347 (2016).
- L. Amirav and A. P. Alivisatos, *J. Phys. Chem. Lett.* **1**, 1051 (2010).
- K. Wu, H. Zhu, Z. Liu, W. Rodríguez-Córdoba, and T. Lian, *J. Am. Chem. Soc.* **134**, 10337 (2012).
- M. Micheel and M. Wächtler (2023). “Dataset for ‘Lateral charge migration in 1D semiconductor-metal hybrid photocatalytic systems,’” Zenodo. [Zenodo.10.5281/zenodo.7680636](https://doi.org/10.5281/zenodo.7680636)